Preprint Title The adsorption of 1-Chloro-1,2,2,2-tetrafluoroethane onto the pristine, Al-, and Ga-doped boron nitride nanosheet

Authors Mohsen Doust Mohammadi and Hewa Y. Abdullah

Publication Date 09 Dez. 2020

Article Type Full Research Paper

ORCID® iDs Mohsen Doust Mohammadi - https://orcid.org/0000-0003-2449-2962; Hewa Y. Abdullah - https://orcid.org/0000-0001-5766-3858

The adsorption of 1-Chloro-1,2,2,2-tetrafluoroethane onto the pristine, Al-, and Ga-doped boron nitride nanosheet

Mohsen Doust Mohammadi[a], Hewa Y. Abdullah[b,*]

[a] *School of Chemistry, College of Science, University of Tehran, Tehran 14176, Iran*

[b] *Physics Education Department, Faculty of Education, Tishk International University, 44001, Erbil, Iraq*

***Corresponding author** Email: hewayaseen@gmail.com

Abstract

DFT were put into practice to study the nature of the intermolecular interactions between 1-Chloro-1,2,2,2-tetrafluoroethane (HCFC-124) gas molecule and pristine, aluminium, and galium doped single-walled boron nitride nanosheets (BNNS). For performing optimization process, various functionals including PBE0, M06-2X, ωB97XD, and B3LYP-D3 were applied on both of the isolated and complex structures. All of the functionals were used together with split-valence triple-zeta basis sets with d-type Cartesian-Gaussian polarization functions (6-311G(d)). To consider the electronic structure, DOS analysis were employed. NBO, QTAIM, and NCI analyses were also taken on board to discover the nature of intermolecular interactions between gas and nanosheets using the same level of theory. The results of electronic structure calculations as well as population analyses has been carefully tabulated and partially depicted. The HOMO-LUMO energy gap was dramatically changed when the dopant atom added to the BNNS. It means the impurity can improve the sensivity and reactivity of the pristine nanosheet; therefore, by absorbing the HCFC-124 onto the surface of the titled nanosheets, a salient signal can produce in a typical electronic circuit. Among all of the absorbents, Al-doped BNNS shows the most favorable material to design a nanosensor for the studied gas molecule.

Keyword: Boron Nitride Nanosheet; 1-Chloro-1,2,2,2-tetrafluoroethane; HCFC-124; Freon 124; Natural Bond Orbital.

1. Introduction

After the emergence of density functional theory (DFT) due to its high computational power for large molecules as well as its considerable accuracy and speed, a suitable framework was provided for the theoretical studies of chemical systems. Many scientists today use this method to understand the properties of chemical structures. Meanwhile, theoretical studies on nanoscale structures have found an extraordinary place in computational chemistry, and researchers have used numerous computational methods to study intermolecular interactions to design tools that have better accuracy and performance [1-5]. A variety of nanomaterials have been considered for the construction of sensors with high measurement accuracy, extreme insensitivity to temperature, very low response time, low production costs, and resistant to harsh environmental conditions [6-12].

Different of methods have been used in theoretical studies to improve the sensitivity of the adsorption process in nanomaterials such as metal doping [13-15], surface defect [16-18], transition metal decoration [19, 20], etc. Impurities introduced to the nanomaterial wall change the energy gap, and also dramatically change its morphology. Lin et al. provides a comprehensive study on the effect of transition metal decoration to boron nitride nanosheet (BNNS) [21]. Studies have shown that even the introduction of non-metals such as oxygen can activate the surface of BNNS [22]. Demonstrating the benefits of dopant element, we can point out that by reducing the electrical resistance, impurity-decorated nanomaterials can generate a stronger signal in the circuit. Therefore, compared to pure nanomaterials, it can be said that decorated nanomaterials have a higher efficiency [23]. Aluminum and gallium are two elements that have been widely used to activate the surface of boron nitride nanosheets in theoretical studies [24-27].

BNNSs are easily synthesized by the chemical vapor deposition method [28]. Due to its remarkable mechanical, thermal, electrical and chemical properties, as well as its excellent reactivity and selectivity, BNNS is widely used [29-31]. The wide band gap (5-6 eV) classified BNNS as an electrical insulator [28, 32, 33]. Ahmadi et al. reported the values of energy gap and B-N bond length for BNNS 5.93 eV and 1.45 Å, respectively, and for Al-doped BNNS the band gap as well as Al-N bond length are 5.39 eVand 1.74 Å, respectively [34]BNNS is also a very successful nanosorbent and has been studied in many theoretical studies to detect H_2O [35] NO [36] , CO [37] , CH_2O [38], $COCl_2$ [39], C_2H_4 [40], and N_2O [41]. This nanosheet and metal decorated BNNS have also been used in the manufacture of many electronic devices [42-48]. It can also be used as a valuable material in the coating industry and metal protection because it is impermeable to gases and liquids and is also an electrical insulator [49-52].

This article encompasses a comprehensive study to investigate the intermolecular interactions of HCFC-124 gas molecule with pristine BNNS plus BN nanosheets doped with Al and Ga. The details information about the computational level was given in section 2. The result and discussion section has been divided in 4 separate subsections: Geometric Surveys (3.1.), which provides insights about bond length and other geometry properties as well as introducing the levels of study for optimizing all structures; Electronic Structure (3.2.) that discusses about DOS and energetic properties results; NBO analysis (3.3.) and QTAIM analysis (3.4) are provided to show the nature of intermolecular interactions between two fragments. We tried to provide a brief theory

for each part using useful references and avoided to bring boring description. And finally, the conclusion section briefly refers to all the findings in this study.

2. Computational details

All of the nanosheet structures were optimized using two-dimensional periodic boundary condition Kohn–Sham density functional theory [53-56] (PBC-DFT) method in vacuum. Various functionals such as PBE0 [57-59], M06-2X [60] , ωB97XD [61] , and B3LYP-D3 scheme of Grimme [62-64] together with split-valence triple-zeta basis sets with d-type Cartesian-Gaussian polarization functions (6-311G(d)) [65-73] were employed through the spin-restricted approach. There is no symmetry constraints were imposed. According to benchmark studies [74], such a basis set covers all we need in this study. A 3×3×1 k point sampling in the Brillouin zone integration [75] with kinetic energy cutoff of 450 eV was hired. In this approach, when the number of unit cells increase the total energy will become minimal. All the molecular geometries were built in Gaussview 6.0.16 [76] software package then fully optimized by the Berny [77] method by Gaussian 16 Rev. C.01 [78] linux based software. The optimization process were performed using the default Gaussian convergence criteria. To configure the stability of each structure frequency calculation were done to determine the nature of the stationary points. In addition, the wave function stability calculation were also done to consider stability of the electrons. Natural bond orbital (NBO) calculations were carried out using the NBO v 3.1 software, which is coupled within Gaussian package to consider the charge-transfer interactions between occupied and unoccupied orbitals. To extract the result data of NBO, NCI, and QTAIM analyses, Multiwfn [79] software was used and GaussSum [80] package depicted the DOS diagrams.

The energy of adsorption (E_{ads}) between two fragments (nanosheet and HCFC-124) can be considered as follows:

$$E_{ads} = E_{sheet/HCFC-124} - E_{sheet} - E_{HCFC-124} + \Delta E_{(BSSE)} \quad (1)$$

where $E_{sheet/HCFC-124}$ shows the total energy of the gas/nanosheet cluster. E_{sheet} and $E_{HCFC-124}$ are the energies of the isolated nanosheet and isolated gas molecule, respectively. Basis set superposition error (BSSE) was obtained from the Boys and Bernardi's counterpoise procedure [81, 82] as follows:

$$\Delta E_{(BSSE)} = \Delta E_{cluster} - \Delta E_{nanosheet}^{cluster} - \Delta E_{gas}^{cluster} \quad (2)$$

According to Equation 1, negative values of E_{ads} (i.e. exothermic adsorptions) indicate that the formed complex is stable; otherwise, positive values of E_{ads} is belong to a local minimum in which the adsorption of HCFC-124 and nanosheet is detered by a energy barrier.

3. Result and discussion

3.1 Geometric Surveys

The PEB0 functional, hybrid form of Perdew–Burke–Ernzerhof (PBE) [57], together with 6-311G(d) basis set were selected at the first stage to start the geometry optimization process of the isolated and complex structures. Although PBE0 is fast, it cannot describe the long-range interactions, dispersion effect, and charge transfer excitations; therefore, all of the structures were re-optimized using robust methods like M06-2X, ωB97XD, and B3LYP-D3. Head-Gordon et al. [61] invented the ωB97XD functional to account for the effect of long-range interactions as well as the dispersion corrections. Among Minnesota 06 suit, which is developed by Truhlar et al. [83]

, the global hybrid functional with double non-local exchange (2X) amounts (i.e. M06-2X) is a high performance method to study the non-covalent interactions. To study the dispersion effect, the latest version of B3LYP-D3 known as D3 (BD) (GD3BJ) developed by Grimme et al. [62-64] would be a good option. In order to compare the effect of each of the mentioned corrections, in Table 1, the amounts of adsorption energy obtained from PBE0 method can be evaluated with other more complex aforementioned methods.

The PBC-DFT framework at PBE0/6-311G(d) level was applied on a pristine $B_{18}N_{18}$ unit cell with 10.004 Å in each dimension. Figure 1 shows the selected boron nitride nanosheet (BNNS). Then the unit cell expanded 3 times along with each axis and the optimization process repeated with the same level of theory. It should be noted that, to reduce the boundary effects, the terminal atoms were terminated by H atoms. For the case for Al and Ga doped nanosheets, after the optimized expanded BNNS obtained, one of the boron atoms substituted by Al or Ga elements and calculations were performed at PBE0/6-311G(d) level of theory. The re-optimization process were performed using 3 other functionals and same basis set. The values of bond length for BNNS, BNAlNS, and BNGaNS are depicted in Figure 2. As is obvious from Figure 2 (a), the B-N bond length is 1.45 Å. Also, Figures 2 (b) and (c) show the value of bond length for Al-N and Ga-N 1.71 Å and 1.74 Å , respectively. Due to the inner stress, the B-N bond length in the vicinity of Al ad Ga dopant atoms vary from 1.42 Å to 1.49 Å.

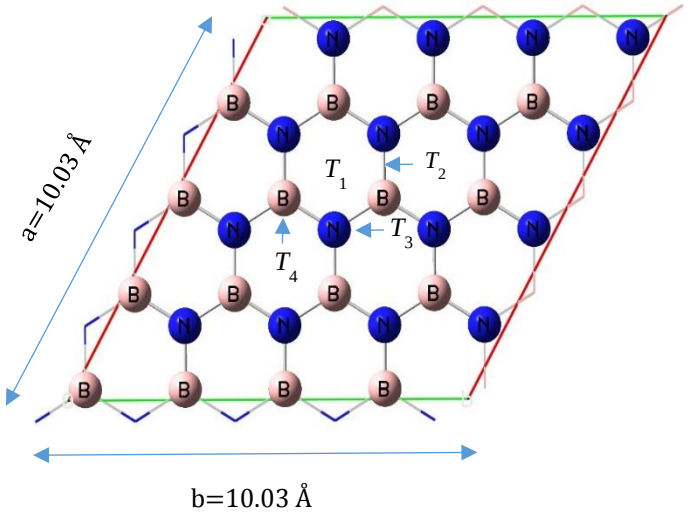

Figure 1: The boron nitride unit cell (32 atoms, 192 electrons, neutral, and singlet) prepared to perform two-dimensional periodic boundary condition density functional theory calculations.

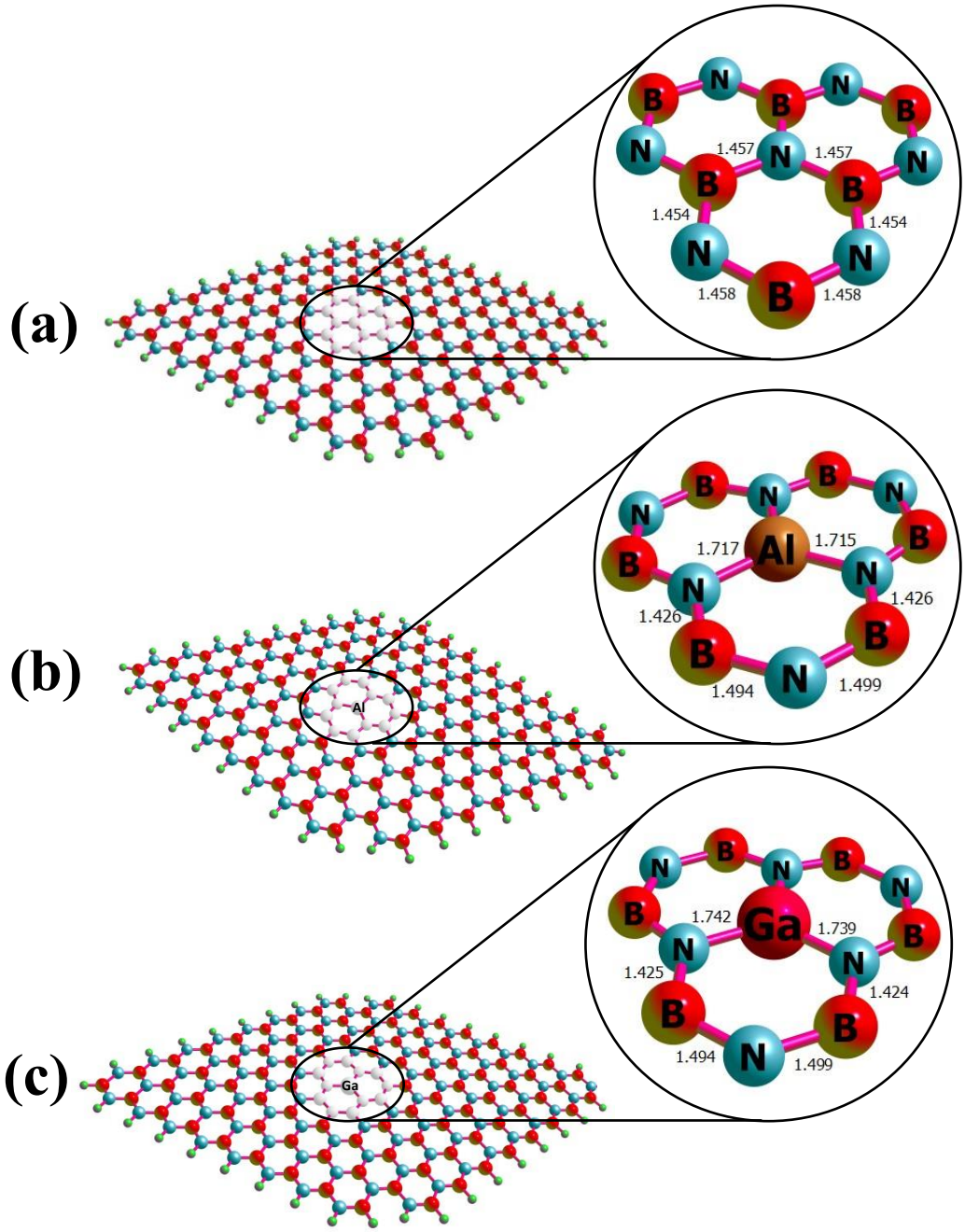

Figure 2: The bond length (Å) obtained at B3LYP-D3/6-311(d) level for **(a)** BNNS, **(b)** BNAlNS, and **(c)** BNGaNS.

The adsorption of HCFC-124 gas molecule onto the surface of pristine and Al, Ga-doped BNNS were also carried out. To achieve this goal, the gas molecule should be placed on top of the nanosheet in different positions through different orientations. The purpose of such calculations is to find energy local minima. Figure 3 shows the different heads of HCFC-124 including H, Cl and different F heads. Carbon atoms are also numbered to be separable in the coming tables. And there are 4 different sites in the BNNS (Figure 1) including: T_1, in the middle of hexagonal ring; T_2, between B and N atoms; T_3, N atom; and T_4, B atom. The gas molecule were put on top of each T_x sites through different distances and optimization process started at PM7/6-311G(d) level. It should be stressed that, overall, there are 240 initial orientations were prepared (i.e. 6×4×10=240. It means 6 different gas molecule heads were put on each of the 4 sites of nanosheet from 0.5 to 5.0 Å vertical distances with 0.5 Å intervals). Right after that, 12 minima were predicted. We select these 12 complex structures to optimize using PBE0/6-311G(d) level of theory. Regarding the values of adsorption energies , finally, the most stable complexes were chosen and re-optimization were done using other functionals including M06-2X, ωB97XD, and B3LYP-D3. The relaxed structures of all complexes which has been obtained from B3LYP-D3/6-311G(d) are depicted in Figure 4. When the values of E_{ads} are "below the range of chemical interest" [84], such results provides identical results.

The adsorption energy obtained from ωB97XD and B3LYP-D3 are closed to each other. The ωB97XD functional shows the most negative Eads values according to Table 1. It seems these two functional are good options for further investigations in this study. The most negative value of Eads is corresponds to the adsorption of gas onto the Al-doped BNNS, -1.586 eV which indicates that the reactivity of HCFC-124 gas is significant. Otherwise, the reactivity of gas and pristine BNNS shows the weakest interaction, among those doped sheets. We preferred to run the population analysis calculations with B3LYP-D3 to reduce the computation times. Therefore, all the interactions analyses were applied to the results of the B3LYP-D3/6-311G(d) level of theory.

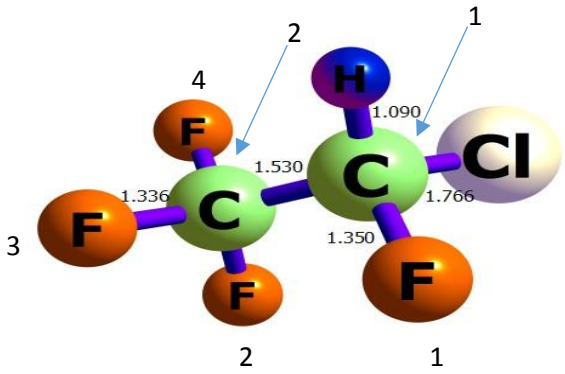

Figure 3: The relaxed structure of 1-Chloro-1,2,2,2-tetrafluoroethane gas molecule obtained from B3LYP-D3/6-311G(d) level of theory.

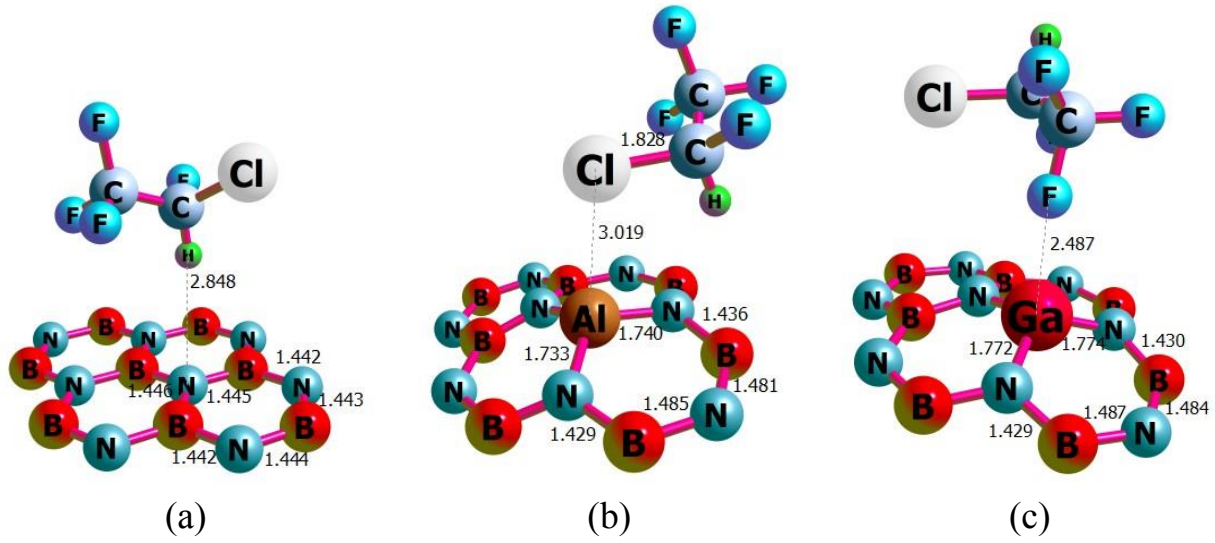

(a) (b) (c)

Figure 4: The relaxed structures of a) HCFC-124/BNNS, b) HCFC-124/BNAlNS, and c) HCFC-124/BNGaNS obtained from B3LYP-D3/6-311G(d) level of theory.

Table1: The adsorption energies (E_{ads}) HCFC-124/nanosheet complexes. All values are in eV and obtained from geometry optimization calculations using PBE0, M06-2X, ωB97XD, and B3LYP-D3 functional in combination with 6-311G(d) basis set.

Systems	PBE0	B3LYP-D3	M06-2X	ωB97XD
C_2HClF_4/BNNS	-0.767	-0.899	-0.776	-1.064
C_2HClF_4/BNAlNS	-1.117	-1.438	-1.126	-1.586
C_2HClF_4/BNGaNS	-1.057	-1.416	-1.207	-1.518

3.2 Electronic Structure

The "Conceptual DFT" has been developed to consider the reactivity concept. Various properties can be obtained from HOMO-LUMO enrgy gap (HLG) [85] in such a way when an external potential apply to a system the energy, in the Hohenberg−Kohn theorems [53] context, changes as follows:

$$\begin{aligned}\Delta E &\equiv E\left[N+\Delta N, v(\mathbf{r})+\Delta v(\mathbf{r})\right]-E\left[N, v(\mathbf{r})\right] \\ &=\left(\frac{\partial E}{\partial N}\right)_v \Delta N+\int\left(\frac{\delta E}{\delta v(\mathbf{r})}\right)_N \delta v(\mathbf{r}) d(\mathbf{r})+ \\ &\frac{1}{2!}\left\{\left(\frac{\partial^2 E}{\partial N^2}\right)_v \Delta N^2+2\int\left(\frac{\partial}{\partial N}\left(\frac{\delta E}{\partial v(\mathbf{r})}\right)_N\right)_v \Delta N \delta v(\mathbf{r})+\int\int\left(\frac{\partial^2 E}{\partial v^2(\mathbf{r})}\right)_N \delta v(\mathbf{r}) \delta v(\mathbf{r}') d\mathbf{r} d\mathbf{r}'\right\}+\ldots\end{aligned} \tag{3}$$

In the above Taylor expansion N is a global quantity and $v(\mathbf{r})$ is a local function. Each term has a specifict meaning in the chemical language as follows:

$$-\chi=\left(\frac{\partial E}{\partial N}\right)_v=\mu \cong \frac{\left(\varepsilon_{LUMO}+\varepsilon_{HOMO}\right)}{2} \tag{4}$$

$$\eta=\left(\frac{\partial \mu}{\partial N}\right)=\frac{1}{2}\left(\frac{\partial^2 E}{\partial N^2}\right)_v=\frac{1}{2}\left(IP-EA\right) \tag{5}$$

$$\omega=\frac{\mu^2}{2\eta} \tag{6}$$

Equation 4 shows the nagative electronegativity (χ) which is equal to chemical potential (μ). Also the values of HOMO and LUMO are related to the ionization affinity and electron affinity, respectively. You can follow the other terms to reach to the Fukui function, response function, dual descriptor, etc [86, 87]. And Equation 6 is related to the electrophilicity index (ω). The values of these properties are listed in Table 2.

The energy gap (E_g) of BNNS has calculated about 5.78 eV at B3LYP-D3/6-311G (d) level of theory and the adsorption of HCFC-124 on it reduced the energy gap to 5.72 which shows although adsorption energy is about -0.9 eV the sensitivity is not significant. On the other hand, Al- and Ga-doped nanosheets meaningfully reduced the E_g values. Table 2 Shows the LUMO values were largely stabilized then the E_g has been reduced. For the case of BNAlNS this reduction of E_g is higher than BNGaNS; therefore, the sensor response (S) is more stronger according to the following equations:

$$S=\left|\left(\frac{\sigma_1}{\sigma_2}\right)-1\right|=\exp\left(\frac{\left|\Delta E_g\right|}{kT}\right)-1 \tag{7}$$

$$\sigma = AT^{3/2}e^{\frac{E_g}{2kT}} \quad (8)$$

Where A is a constant and σ is electrical conductivity, k is Boltzmann's constant, and T is Kelvin temperature. The resistivity will be diminished when Eg is being reduced, since the resistivity is proportional to the reciprocal of the conducting electron population. Hence, the resistivity for BNAlNS/gas adsorption is low and the electric current generated in the circuit will face the lowest resistance. Density of state (DOS) map is useful in intuitively revealing density of distribution of molecular orbitals in different energy regions, and gap is directly visible from this map (Figure 5).

Table 2: HOMO energy (ε_H), LUMO energy (ε_L), Fermi energy (E_F), HOMO–LUMO energy gap (HLG), chemical potential (μ), chemical hardness (η), and electrophilicity (ω). All values are in eV and were obtained using the B3LYP-D3/6-311G (d) level of theory.

Systems	ε_H	ε_L	E_F	HLG	μ	η	ω
BNNS	-6.474	-0.695	-3.584	5.778	-3.584	2.889	18.560
BNAlNS	-6.389	-0.686	-3.538	5.703	-3.538	2.851	17.841
BNGaNS	-6.391	-0.687	-3.539	5.705	-3.539	2.852	17.862
C_2HClF_4/BNNS	-6.386	-0.664	-3.525	5.721	-3.525	2.861	17.772
C_2HClF_4/BNAlNS	-6.389	-1.520	-3.955	4.869	-3.955	2.435	19.037
C_2HClF_4/BNGaNS	-6.305	-1.260	-3.782	5.045	-3.782	2.523	18.043

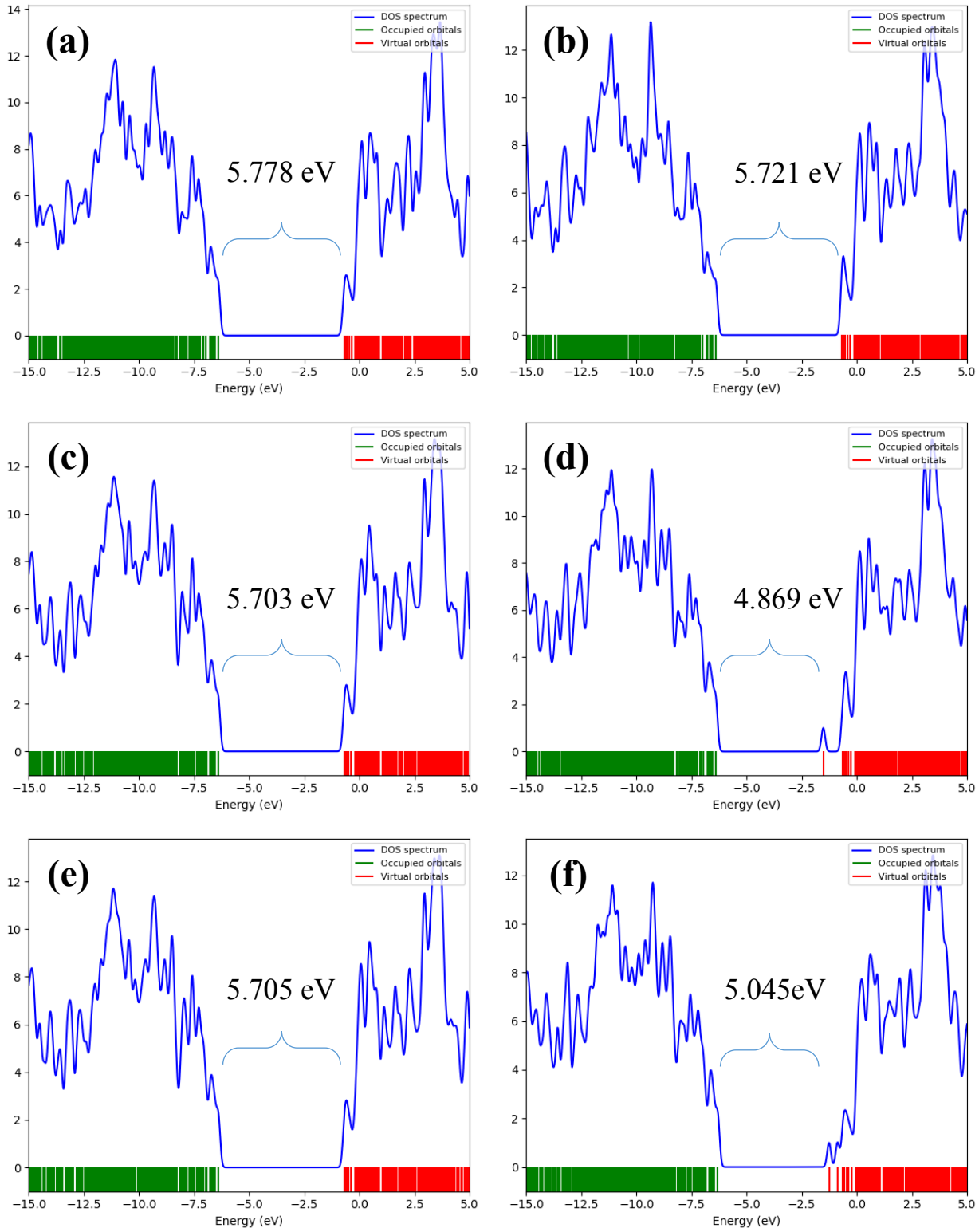

Figure 5: Density of state maps for (a) BNNS (b) HCFC-124/BNNS (c) BNAlNS (d) HCFC-124/BNAlNS (e) BNGaNS (f) HCFC-124/BNGaNS. Data were obtained from the B3LYP-D3/6-311G (d) level of theory

3.3 NBO Analysis

The Natural bond orbital (NBO) method, developed by Weinhold et al. [88-90], is one of the most respectful population analyses and uses to calculate the distribution of electron density in bonds between atoms. The term NBO refers to a bonding orbital with the maximum electron density. A density matrix, calculated from DFT, as well as atomic charge, are used to define natural bonding orbitals. To complete the span of valance space in addition to bonding NBO (σ), we need an antibonding NBO (σ*) as follows:

$$\sigma_{AB} = C_A h_A + C_B h_B \tag{9}$$

$$\sigma^*_{AB} = C_A h_A - C_B h_B \tag{10}$$

where h_A and h_B are natural hybrid valance orbitals, C_A and C_B are the corresponding polarization coefficients. In the present study, NBO calculations were performed to figure out various types of bond order including Mulliken [91](Equation 11) and Mayerb [92-94] (Equation 12) bond order as well as Wiberg bond index (WBI) in Löwdin orthogonalized basis [95, 96] (Equation 13). Thus,

$$I_{AB} = \sum_i \eta_i \sum_{a\in A}\sum_{b\in B} 2C_{a,i}C_{b,i}S_{a,b} = 2\sum_{a\in A}\sum_{b\in B} P_{a,b}S_{a,b} \tag{11}$$

$$I_{AB} = I^{\alpha}_{AB} + I^{\beta}_{AB} = 2\sum_{a\in A}\sum_{b\in B}\left[\left(P^{\alpha}S\right)_{ba}\left(P^{\alpha}S\right)_{ab} + \left(P^{\beta}S\right)_{ba}\left(P^{\beta}S\right)_{ab}\right] \tag{12}$$

$$I_{AB} = \sum_{a\in A}\sum_{b\in B} P^2_{ab} \tag{13}$$

In the above Equations, P and S are density and overlap matrix, respectively. Mulliken and Mayer's bond orders are sensitive to the basis set, spacially for the basis set including diffuse functions. On the other hand, Wiberg bond order with respect to the two other is less basis set dependence. Table 3 reports the values of obtained bond orders from different methods. According to the WBI which is more accurate than Mayer and Mulliken we can up to this conclusion that BNAlNS adsorbent is the most material in this study for adsorbing HCFC-124. The bond order value shows that the interaction of gas with BNNS can be classified as physisorption; otherwise, the interactions between Al and Ga-doped BNNS with the gas molecules are more significant.

In addition, natural charges and natural electron configuration data were obtained. Using NBO consideration the nature of intermolecular interaction between HCFC-124 gas molecule and nanosheets becomes more understandable. According to Table 4, the charge transfer is obvious. The valance shell of F atom was changed from 2p(5.50) to 2p(5.49)3d(0.01) during the adsorption process. It means strong interaction has occurred.

Table 3: The values of Mulliken, Mayer, and Wiberg bond order obtained from the interactions of the HCFC-124 molecule and BNNS, BNAlNS, and BNGaNS. All calculations were performed using the B3LYP-D3/6-311G (d) level of theory.

Systems	X[a]....Y[b]	Mulliken	Mayer	WBI
C_2HClF_4/BNNS	H.....N	0.290	0.022	0.005
C_2HClF_4/BNAlNS	Cl....Al	0.060	0.115	0.254
C_2HClF_4/BNGaNS	F....Ga	0.102	0.124	0.244

(a) X atoms are belong to HCFC-124
(b) Y atoms are belong to Nanosheets

Table 4: The values of natural charges (au) and Natural electron configurations for the isolated HCFC-124, and its complex structures. All values were calculated using the B3LYP-D3/6-311G (d) level of theory.

Systems	atom	Natural Charge	Natural Electron Configuration
C_2HClF_4	C1	1.06	[core]2S(1.03)2p(2.76)3S(0.01)3p(0.02)3d(0.01)
	C2	0.16	[core]2S(0.76)2p(2.11)3p(0.04)3d(0.02)
	H	0.18	1S(0.81)
	Cl	-0.02	[core]3S(1.86)3p(5.15)3d(0.01)4p(0.01)
	F1	-0.34	[core]2S(1.84)2p(5.50)
	F2	-0.35	[core]2S(1.84)2p(5.50)
	F3	-0.34	[core]2S(1.84)2p(5.49)
	F4	-0.35	[core]2S(1.84)2p(5.50)
C_2HClF_4/BNNS	C1	1.06	[core]2S(0.78)2p(2.08)3p(0.03)3d(0.02)
	C2	0.18	[core]2S(1.03)2p(2.76)3S(0.01)3p(0.02)3d(0.01)
	H	0.19	1S(0.80)
	Cl	-0.04	[core]3S(1.88)3p(5.12)3d(0.01)4p(0.01)
	F1	-0.35	[core]2S(1.85)2p(5.49)3d(0.01)
	F2	-0.35	[core]2S(1.85)2p(5.49)3d(0.01)
	F3	-0.35	[core]2S(1.85)2p(5.49)3d(0.01)
	F4	-0.35	[core]2S(1.85)2p(5.49)3d(0.01)
C_2HClF_4/BNAlNS	C1	1.07	[core]2S(0.78)2p(2.08)3p(0.03)3d(0.02)
	C2	0.17	[core]2S(1.03)2p(2.76)3S(0.01)3p(0.02)3d(0.01)
	H	0.21	1S(0.80)
	Cl	-0.01	[core]3S(1.88)3p(5.12)3d(0.01)4p(0.01)
	F1	-0.34	[core]2S(1.85)2p(5.49)3d(0.01)
	F2	-0.34	[core]2S(1.85)2p(5.49)3d(0.01)
	F3	-0.35	[core]2S(1.85)2p(5.49)3d(0.01)
	F4	-0.36	[core]2S(1.85)2p(5.49)3d(0.01)
C_2HClF_4/BNGaNS	C1	1.07	[core]2S(0.78)2p(2.08)3p(0.03)3d(0.02)
	C2	0.17	[core]2S(1.03)2p(2.76)3S(0.01)3p(0.02)3d(0.01)
	H	0.20	1S(0.80)

Cl	-0.01	[core]3S(1.88)3p(5.12)3d(0.01)4p(0.01)
F1	-0.34	[core]2S(1.85)2p(5.49)3d(0.01)
F2	-0.34	[core]2S(1.85)2p(5.49)3d(0.01)
F3	-0.35	[core]2S(1.85)2p(5.49)3d(0.01)
F4	-0.34	[core]2S(1.85)2p(5.49)3d(0.01)

3.4 QTAIM Analysis

QTAIM analysis is used study bond types and intermolecular interactions. A critical point of the electron density, including minimum, maximum, or saddle point, can belong to: (1) *Atomic critical point* (ACP); (2) *bond critical point* (BCP); (3) *ring critical point* (RCP); and (4) *cage critical point* (CCP). The Electron density $\rho(\mathbf{r})$ and the Laplacian electron density $\nabla^2\rho(\mathbf{r})$ are playing important role in the QTAIM analysis since they determine the segmentation and identification of different types of chemical interactions. A bond critical point with negative values of Laplacian electron density and large values of electron density ($\rho(\mathbf{r})>10^{-1}$ a.u.) is defined as a covalent bond. On the other hand, the positive value of $\nabla^2\rho(\mathbf{r})$ designates that the interactions can be classified as of the non-substrate close-shell type (which include ionic and van der Waals interactions) [97].

The values of Lagrangian kinetic energy $G(\mathbf{r})$ and potential energy density $V(\mathbf{r})$ divulges the nature of the intermolecular interaction; therefore, the ratio of $G(\mathbf{r})/|V|(\mathbf{r})$ can be hired as an appropriate index in link classification. When $G(\mathbf{r})/|V|(\mathbf{r})<0.5$, the nature of the interaction is covalent, and if $G(\mathbf{r})/|V|(\mathbf{r})>1$, the interaction is non-covalent. Large values of elliptical bond (ε) represents an unstable structure and defined as follows [98] :

$$\varepsilon = \frac{\lambda_1}{\lambda_2} - 1 \ , |\lambda_1| > |\lambda_2| \tag{14}$$

According to virial theorem [99], a relationship exists between $G(\mathbf{r})$, $V(\mathbf{r})$, and $\nabla^2\rho(\mathbf{r})$ as follows:

$$\frac{1}{4}\nabla^2\rho(\mathbf{r}) = 2G(\mathbf{r}) + V(\mathbf{r}) \tag{15}$$

From Table 5 all values for $\nabla^2\rho(\mathbf{r})$ are positive. except Cl....Al interaction between HCFC-124 and BNAlNS, the other values of $G(\mathbf{r})/|V|(\mathbf{r})$ are higher than 1. These results shows intermolecular interactions are classified as non-covalent. In the case of BNAlNS very strong interactions were observed. And finally the small values of ε shows that all of the structures are stable.

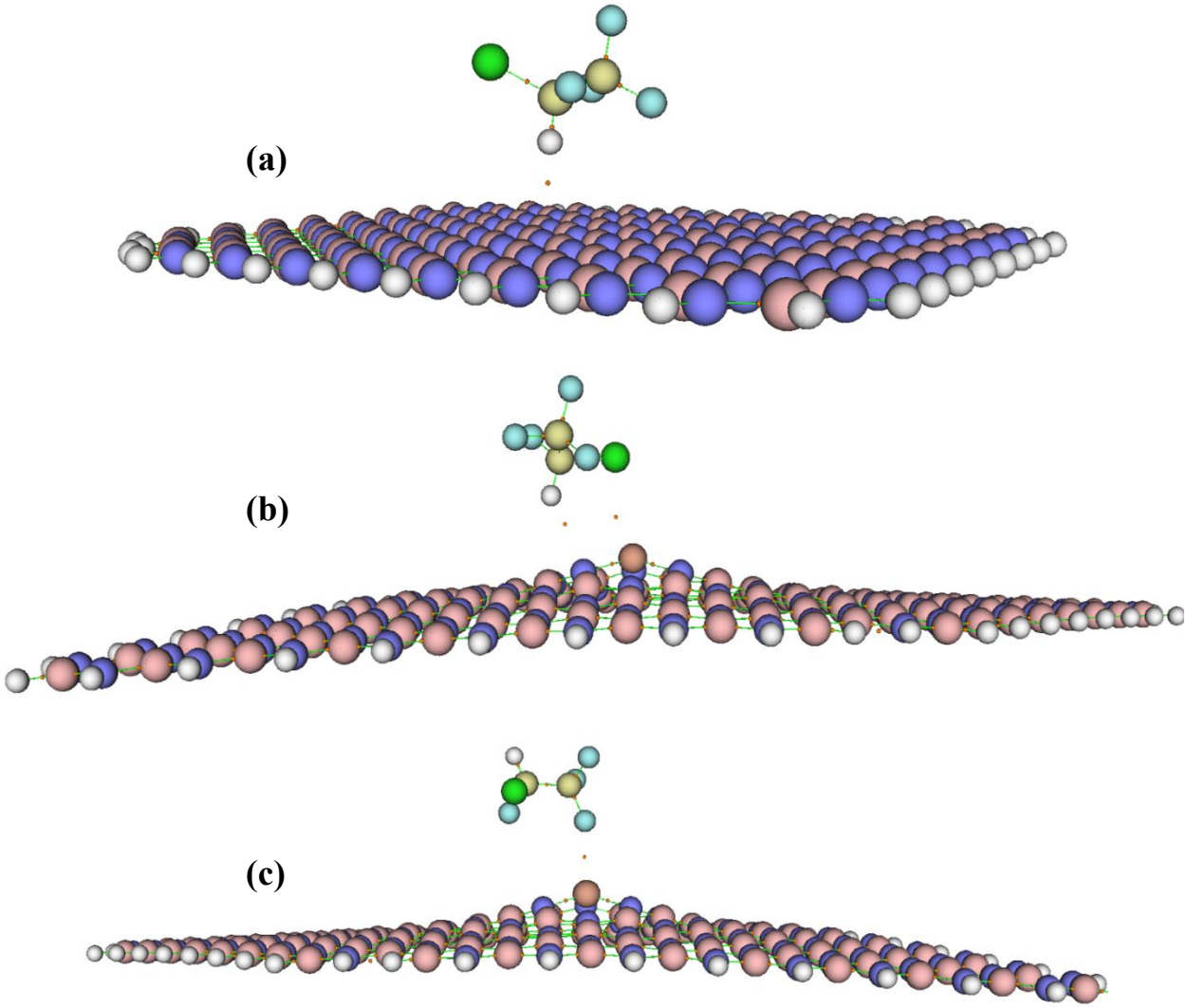

Figure 6: The Bond Critical points graphs for the (a) HCFC-124/BNNS, (b) HCFC-124/BNAlNS, (c) and HCFC-124/BNGaNS systems. The orange dots represent the BCPs

Table 5: QTAIM topological parameters for electron density ρ(r), Laplacian of electron density $\nabla^2\rho$(r), kinetic electron density G(r), potential electron density V(r), eigenvalues of Hessian matrix (λ), and bond ellipticity index (ε) at the BCPs of the HCFC-124 clusters with BNNS, BNAlNS, and BNGaNS. All values were calculated using the B3LYP-D3/6-311G (d) level of theory and NBO analysis.

Systems	Bond	ρ	$\nabla^2 r$	G(r)	V(r)	G(r)/V(r)	λ_1	λ_2	λ_3	ε
C_2HClF_4/BNNS	H....B	0.0057	0.0179	0.0037	-0.0029	1.2781	-0.0021	-0.0038	0.0238	0.7598
C_2HClF_4/BNAlNS	H....N	0.0121	0.0371	0.0079	-0.0066	1.2076	-0.0100	-0.0105	0.0577	0.0501
	Cl....Al	0.0121	0.0195	0.0053	-0.0058	0.9227	-0.0051	-0.0078	0.0324	0.5138
C_2HClF_4/BNGaNS	F....Ga	0.0193	0.0796	0.0195	-0.0190	1.0220	-0.0163	-0.0171	0.1130	0.0504

The results of QTAIM, in the previous section, showed that the interactions between HCFC-124 and nanosheets are non-covalent; hence, it is useful to check them by a non-covalent analysis. Reduced density gradient (RDG) and sign$\lambda_2(r)\rho(r)$ are a pair of functions used in non-covalent interaction (NCI) [100] analysis which can be implemented to visualize the region and the type of weak interactions. RDG is defined as follows [100, 101]:

$$\mathrm{RDG} = \frac{1}{2(3\pi^2)^{\frac{1}{3}}} \frac{\left|\overline{\Delta\rho}(\mathbf{r})\right|}{\overline{\rho(\mathbf{r})}^{\frac{4}{3}}} \tag{16}$$

The two functions RDG and sign$\lambda_2(\mathbf{r})\rho(\mathbf{r})$ can be plotted to define specific areas. In this case, non-covalent interactions will be identified. The points that indicate strong interactions are located in the sign$\lambda_2(\mathbf{r})\rho(\mathbf{r}) < 0$ region. Relatively weak van der Waals interactions are found in the sign$\lambda_2(\mathbf{r})\rho(\mathbf{r}) \approx 0$ region. And if points are in sign$\lambda_2(\mathbf{r})\rho(\mathbf{r}) > 0$ region, it means that the interactions are of the type of repulsive [100, 101]. As it turns out, bond strength is closely related to the density matrix $\rho(\mathbf{r})$ as well as signλ_2. Low RDG and low electron density regions should be consulted to determine whether non-covalent interactions occur between the two components involved in the adsorption process.

Considering an isosurface as a reference (e.g. RDG = 0.5), it can be seen that the spots are appeared in the sign$\lambda_2(r)\rho(r) \approx 0$ zone after the adsorption of HCFC-124 molecule onto BNNS and BNGaNS; therefore, the interactions can classified as van der Waals. However, the interactions of HCFC-124 with BNAlNS were strong in nature. NCI analysis also confirms the results of the adsorption energy calculations, QTAIM analysis, and NBO analysis, namely that the interactions of HCFC-124 with the Al and Ga-doped BNNS were strong.

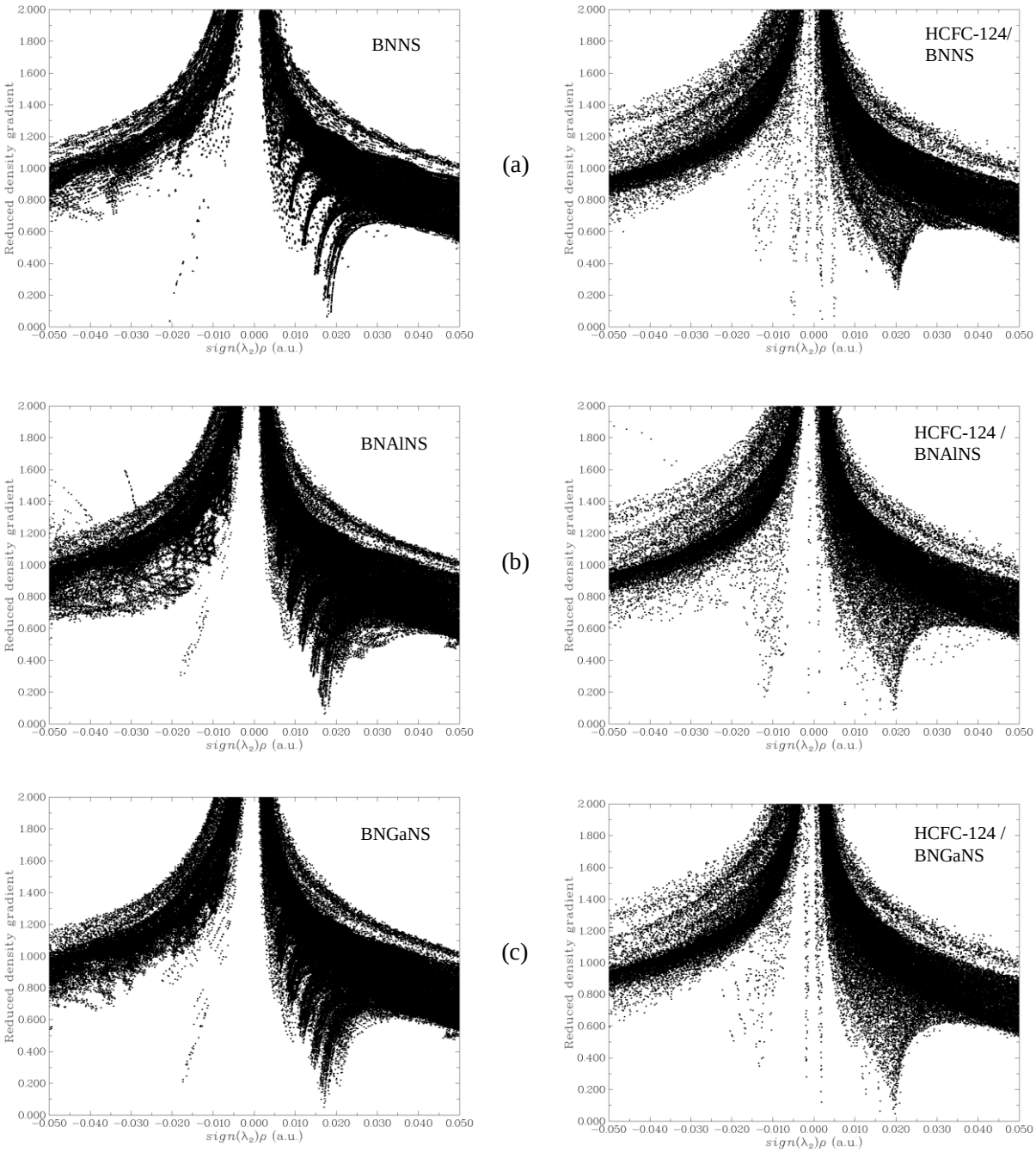

Figure 7: The RDG vs. sign(λ_2)ρ(r) diagrams for (a) pristine (b) Al-doped, and (c) Ga-doped BNNSs. The diagrams were obtained from B3LYP-D3/6-311G(d) level of theory. Left panel shows isolated nanosheets and right panel shows HCFC-124/nanosheet complexes.

4. Conclusion

The intermolecular interactions between the HCFC-124 gas molecule and BNNS, BNAlNS, and BNGaNS were studied by the DFT framework in vacuum condition. All molecular structures optimized at PBE0, M06-2X, ωB97XD, and B3LYP-D3 functionals together with a 6-311G(d) basis set. Relaxed structures obtained from B3LYP-D3/6-311G(d) were chosen for population analysis calculations. Results of adsorption energy show that among the nanosheets, the interaction of BNAlNS and gas (about -1.59 eV) is higher than the other adsorbents. DOS analysis can also approve that the most reduction of energy gap (about 0.83 eV) is related to the gas/BNAlNS cluster. Different bond order analysis data repeats former results. To shed light on the nature of intermolecular interactions NBO QTAIM, and NCI analyses were implemented and the results of all the analyses were in agreement. From NBO analysis, the charge transfer was observed and NCI and QTAIM results show strong intermolecular interactions-specially for BNAlNS/gas cluster. To sum up, we can conclude injecting Al and Ga elements inside the BNNS can dramatically active its surface in favor of adsorbing HCFC-124 gas. Accordingly, these nanomaterials would be favorable for designing a sensitive nanosensor.

Conflict of Interest

The authors declare no conflict of interest

Acknowledgements

I would like to thank the Solid-State Theory Group at the Physics Department at the Universita‘ degli Studi di Milano-Italy for providing computational facilities.

References

[1] R. Dos Santos, R. Rivelino, F. de Brito Mota, G. Gueorguiev, and A. Kakanakova-Georgieva. *Journal of Physics D: Applied Physics*. **2015**, 48, (29), 295104.

[2] M. D. Mohammadi, and M. Hamzehloo. *Computational and Theoretical Chemistry*. **2018**, 1144, 26-37.

[3] H. Ghafur Rauf, S. Majedi, E. Abdulkareem Mahmood, and M. Sofi. *Chemical Review and Letters*. **2019**, 2, (3), 140-150.

[4] M. Kamel, A. Morsali, H. Raissi, and K. Mohammadifard. *Chemical Review and Letters*. **2020**, 3, (1), 23-37.

[5] F. Li, and H. Asadi. *Journal of Molecular Liquids*. **2020**, 113139.

[6] E. Nemati-Kande, M. Abbasi, and M. Doust Mohammadi. *ChemistrySelect*. **2018**, 3, (34), 9833-9840.

[7] E. Nemati-Kande, M. Abbasi, and M. D. Mohammadi. *ChemistrySelect*. **2019**, 4, (8), 2453-2462.

[8] M. D. Mohammadi, and H. Y. Abdullah. *Journal of Molecular Modeling*. **2020**, 26, (10), 1-15.

[9] M. D. Mohammadi, and H. Y. Abdullah. *Theoretical Chemistry Accounts*. **2020**, 139, (10), 1-17.

[10] M. D. Mohammadi, and H. Y. Abdullah. *Structural Chemistry*. **2020**, 1-14.

[11] M. D. Mohammadi, I. H. Salih, and H. Y. Abdullah. *Journal of Computational Biophysics and Chemistry*. **2020**, 1-17.

[12] E. Nemati-Kande, M. Abbasi, and M. D. Mohammadi. *Journal of Molecular Structure*. **2020**, 1199, 126962.

[13] K. Wilke, and H. Breuer. *Journal of Photochemistry and Photobiology A: Chemistry*. **1999**, 121, (1), 49-53.

[14] D. Saha, and S. Deng. *Langmuir*. **2009**, 25, (21), 12550-12560.

[15] J. A. Botas, G. Calleja, M. Sánchez-Sánchez, and M. G. Orcajo. *Langmuir*. **2010**, 26, (8), 5300-5303.

[16] L.-Q. Wang, D. R. Baer, M. H. Engelhard, and A. N. Shultz. *Surface science*. **1995**, 344, (3), 237-250.

[17] K. Bolton. *Journal of Molecular Structure: THEOCHEM*. **2003**, 632, (1-3), 145-156.

[18] Z. Wu, M. Li, J. Howe, H. M. Meyer III, and S. H. Overbury. *Langmuir*. **2010**, 26, (21), 16595-16606.

[19] T. Yildirim, J. Íñiguez, and S. Ciraci. *Physical Review B*. **2005**, 72, (15), 153403.

[20] K. Srinivasu, and S. K. Ghosh. *The Journal of Physical Chemistry C*. **2012**, 116, (48), 25184-25189.

[21] S. Lin, X. Ye, R. S. Johnson, and H. Guo. *The Journal of Physical Chemistry C*. **2013**, 117, (33), 17319-17326.

[22] W. Lei, H. Zhang, Y. Wu, B. Zhang, D. Liu, S. Qin, Z. Liu, L. Liu, Y. Ma, and Y. Chen. *Nano Energy*. **2014**, 6, 219-224.

[23] M. Hjiri, L. El Mir, S. Leonardi, A. Pistone, L. Mavilia, and G. Neri. *Sensors and Actuators B: Chemical*. **2014**, 196, 413-420.

[24] A. A. Darwish, M. M. Fadlallah, A. Badawi, and A. A. Maarouf. *Applied Surface Science*. **2016**, 377, 9-16.

[25] A. Seif, and K. Azizi. *RSC advances*. **2016**, 6, (6), 5079-5088.

[26] A. Seif, and K. Azizi. *RSC advances*. **2016**, 6, (63), 58458-58468.

[27] M. D. Esrafili, and S. Asadollahi. *Journal of Molecular Graphics and Modelling*. **2018**, 85, 323-330.

[28] Y. Lin, and J. W. Connell. *Nanoscale*. **2012**, 4, (22), 6908-6939.

[29] V. Guerra, C. Wan, and T. McNally. *Progress in Materials Science*. **2019**, 100, 170-186.

[30] J.-l. Li, J.-h. Yin, T. Ji, Y. Feng, Y.-y. Liu, H. Zhao, Y.-p. Li, C.-c. Zhu, D. Yue, and B. Su. *Materials Letters*. **2019**, 234, 74-78.

[31] X. Yang, Y. Guo, Y. Han, Y. Li, T. Ma, M. Chen, J. Kong, J. Zhu, and J. Gu. *Composites Part B: Engineering*. **2019**, 175, 107070.
[32] L. H. Li, and Y. Chen. *Advanced Functional Materials*. **2016**, 26, (16), 2594-2608.
[33] A. Falin, Q. Cai, E. J. Santos, D. Scullion, D. Qian, R. Zhang, Z. Yang, S. Huang, K. Watanabe, and T. Taniguchi. *Nature communications*. **2017**, 8, (1), 1-9.
[34] A. A. Peyghan, M. Noei, and S. Yourdkhani. *Superlattices and Microstructures*. **2013**, 59, 115-122.
[35] R. Omidirad, and K. Azizi. *Journal of Molecular Graphics and Modelling*. **2019**, 93, 107448.
[36] M. D. Esrafili, and N. Saeidi. *Applied Surface Science*. **2018**, 444, 584-589.
[37] M. D. Esrafili. *Chemical Physics Letters*. **2018**, 695, 131-137.
[38] M. D. Esrafili, P. Mousavian, and F. A. Rad. *Journal of Molecular Graphics and Modelling*. **2018**, 82, 101-107.
[39] R. Moladoust, M. D. Esrafili, A. Hosseinian, I. Alkorta, and E. Vessally. *Molecular Physics*. **2019**, 117, (5), 626-634.
[40] M. D. Esrafili. *Solid State Communications*. **2018**, 284, 35-39.
[41] M. D. Esrafili, S. Asadollahi, and S. Heydari. *Journal of Molecular Graphics and Modelling*. **2019**, 89, 41-49.
[42] H. Li, Z. Chen, X. Fang, and D. Tie. *Superlattices and Microstructures*. **2015**, 88, 371-376.
[43] S. Lin, J. Huang, and X. Gao. *Physical Chemistry Chemical Physics*. **2015**, 17, (34), 22097-22105.
[44] J. Azamat, A. Khataee, and S. W. Joo. *Journal of Molecular Structure*. **2016**, 1108, 144-149.
[45] M. D. Esrafili, N. Saeidi, and P. Nematollahi. *New Journal of Chemistry*. **2016**, 40, (9), 8024-8031.
[46] M. D. Esrafili, and N. Saeidi. *International Journal of Quantum Chemistry*. **2017**, 117, (24), e25450.
[47] Z. Ai, B. Chang, C. Xu, B. Huang, Y. Wu, X. Hao, and Y. Shao. *New Journal of Chemistry*. **2019**, 43, (22), 8613-8619.
[48] R. W. Dorn, M. J. Ryan, T.-H. Kim, T. W. Goh, A. Venkatesh, P. M. Heintz, L. Zhou, W. Huang, and A. J. Rossini. *Chemistry of Materials*. **2020**, 32, (7), 3109-3121.
[49] L. H. Li, T. Xing, Y. Chen, and R. Jones. *Advanced materials interfaces*. **2014**, 1, (8), 1300132.
[50] L. Fu, G. Chen, N. Jiang, J. Yu, C.-T. Lin, and A. Yu. *Journal of Materials Chemistry A*. **2016**, 4, (48), 19107-19115.
[51] W. Luo, Y. Wang, E. Hitz, Y. Lin, B. Yang, and L. Hu. *Advanced Functional Materials*. **2017**, 27, (31), 1701450.
[52] M. A. Raza, A. Nadeem, and M. T. Ilyas. "Corrosion Study of Boron Nitride Nanosheets Deposited on Copper Metal by Electrophoretic Deposition." pp. 681-685.
[53] P. Hohenberg, and W. Kohn. *Physical review*. **1964**, 136, (3B), B864.
[54] W. Kohn, and L. J. Sham. *Physical review*. **1965**, 140, (4A), A1133.
[55] J. A. Pople, P. M. Gill, and B. G. Johnson. *Chemical physics letters*. **1992**, 199, (6), 557-560.
[56] F. M. Bickelhaupt, and E. J. Baerends. *Reviews in computational chemistry*. **2000**, 15, 1-86.
[57] J. P. Perdew, K. Burke, and M. Ernzerhof. *Physical review letters*. **1996**, 77, (18), 3865.
[58] J. P. Perdew, M. Ernzerhof, and K. Burke. *The Journal of chemical physics*. **1996**, 105, (22), 9982-9985.
[59] C. Adamo, and V. Barone. *The Journal of chemical physics*. **1999**, 110, (13), 6158-6170.
[60] Y. Zhao, and D. G. Truhlar. *Theoretical Chemistry Accounts*. **2008**, 120, (1-3), 215-241.
[61] J.-D. Chai, and M. Head-Gordon. *Physical Chemistry Chemical Physics*. **2008**, 10, (44), 6615-6620.
[62] S. Grimme. *Journal of computational chemistry*. **2006**, 27, (15), 1787-1799.
[63] S. Grimme, J. Antony, S. Ehrlich, and H. Krieg. *The Journal of chemical physics*. **2010**, 132, (15), 154104.
[64] S. Grimme, S. Ehrlich, and L. Goerigk. *Journal of computational chemistry*. **2011**, 32, (7), 1456-1465.

[65] P. J. Hay. *The Journal of Chemical Physics*. **1977**, 66, (10), 4377-4384.
[66] R. Krishnan, J. S. Binkley, R. Seeger, and J. A. Pople. *The Journal of chemical physics*. **1980**, 72, (1), 650-654.
[67] M. J. Frisch, J. A. Pople, and J. S. Binkley. *The Journal of chemical physics*. **1984**, 80, (7), 3265-3269.
[68] K. Raghavachari, and G. W. Trucks. *The Journal of chemical physics*. **1989**, 91, (2), 1062-1065.
[69] R. Binning Jr, and L. Curtiss. *Journal of Computational Chemistry*. **1990**, 11, (10), 1206-1216.
[70] M. P. McGrath, and L. Radom. *The Journal of chemical physics*. **1991**, 94, (1), 511-516.
[71] T. V. Russo, R. L. Martin, and P. J. Hay. *The Journal of chemical physics*. **1994**, 101, (9), 7729-7737.
[72] L. A. Curtiss, M. P. McGrath, J. P. Blaudeau, N. E. Davis, R. C. Binning Jr, and L. Radom. *The Journal of Chemical Physics*. **1995**, 103, (14), 6104-6113.
[73] J.-P. Blaudeau, M. P. McGrath, L. A. Curtiss, and L. Radom. *The Journal of chemical physics*. **1997**, 107, (13), 5016-5021.
[74] L. Goerigk, and S. Grimme. *Physical Chemistry Chemical Physics*. **2011**, 13, (14), 6670-6688.
[75] H. Ibach, and H. Lüth. *Solid State and Physics, Springer, Berlin*. **1995**, 244.
[76] R. Dennington, T. A. Keith, and J. M. Millam. *Semichem Inc. Shawnee Mission KS*. **2016**,
[77] J. Baker. *Journal of computational chemistry*. **1987**, 8, (5), 563-574.
[78] M. Frisch, G. Trucks, H. Schlegel, G. Scuseria, M. Robb, J. Cheeseman, G. Scalmani, V. Barone, G. Petersson, and H. Nakatsuji, "Gaussian 16," Gaussian, Inc. Wallingford, CT, 2016.
[79] T. Lu, and F. Chen. *Journal of computational chemistry*. **2012**, 33, (5), 580-592.
[80] N. M. O'boyle, A. L. Tenderholt, and K. M. Langner. *Journal of computational chemistry*. **2008**, 29, (5), 839-845.
[81] S. F. Boys, and F. Bernardi. *Molecular Physics*. **1970**, 19, (4), 553-566.
[82] I. Alkorta, C. Trujillo, J. Elguero, and M. Solimannejad. *Computational and Theoretical Chemistry*. **2011**, 967, (1), 147-151.
[83] F. Ma, Z.-R. Li, Z.-J. Zhou, D. Wu, Y. Li, Y.-F. Wang, and Z.-S. Li. *The Journal of Physical Chemistry C*. **2010**, 114, (25), 11242-11247.
[84] J. Foresman, and E. Frisch. *Gaussian Inc., Pittsburgh, Pennsylvania*. **1996**,
[85] J.-L. Bredas. *Materials Horizons*. **2014**, 1, (1), 17-19.
[86] P. Geerlings, F. De Proft, and W. Langenaeker. *Chemical reviews*. **2003**, 103, (5), 1793-1874.
[87] S.-B. Liu. *Acta Physico-Chimica Sinica*. **2009**, 25, (3), 590-600.
[88] a. J. Foster, and F. Weinhold. *Journal of the American Chemical Society*. **1980**, 102, (24), 7211-7218.
[89] F. Weinhold, and C. R. Landis. *Chemistry Education Research and Practice*. **2001**, 2, (2), 91-104.
[90] F. Weinhold, *Discovering chemistry with natural bond orbitals*: John Wiley & Sons, 2012.
[91] R. S. Mulliken. *The Journal of Chemical Physics*. **1955**, 23, (10), 1833-1840.
[92] I. Mayer. *Chemical Physics Letters*. **1983**, 97, (3), 270-274.
[93] A. J. Bridgeman, G. Cavigliasso, L. R. Ireland, and J. Rothery. *Journal of the Chemical Society, Dalton Transactions*. **2001**, (14), 2095-2108.
[94] I. Mayer. *Chemical Physics Letters*. **2012**, 544, 83-86.
[95] K. B. Wiberg. *Tetrahedron*. **1968**, 24, (3), 1083-1096.
[96] O. V. Sizova, L. V. Skripnikov, and A. Y. Sokolov. *Journal of Molecular Structure: THEOCHEM*. **2008**, 870, (1-3), 1-9.
[97] C. F. Matta, "Hydrogen–Hydrogen Bonding: The Non-Electrostatic Limit of Closed-Shell Interaction Between Two Hydro," *Hydrogen Bonding—New Insights*, pp. 337-375: Springer, 2006.
[98] H. J. Bohórquez, R. J. Boyd, and C. F. Matta. *The Journal of Physical Chemistry A*. **2011**, 115, (45), 12991-12997.

563 [99] S. J. Grabowski. *The Journal of Physical Chemistry A*. **2012**, 116, (7), 1838-1845.
564 [100] E. R. Johnson, S. Keinan, P. Mori-Sánchez, J. Contreras-García, A. J. Cohen, and W. Yang. *Journal*
565 *of the American Chemical Society*. **2010**, 132, (18), 6498-6506.
566 [101] J. Contreras-García, E. R. Johnson, S. Keinan, R. Chaudret, J.-P. Piquemal, D. N. Beratan, and W.
567 Yang. *Journal of chemical theory and computation*. **2011**, 7, (3), 625-632.

568